

Depth analysis of boron diffusion in MgO/CoFeB bilayer by x-ray photoelectron spectroscopy

Yuan Lu, B. Lépine, G. Jezequel, S. Ababou, M. Alnot, J. Lambert, A. Renard, M. Mullet, C. Deranlot, H. Jaffres, et al.

▶ **To cite this version:**

Yuan Lu, B. Lépine, G. Jezequel, S. Ababou, M. Alnot, et al.. Depth analysis of boron diffusion in MgO/CoFeB bilayer by x-ray photoelectron spectroscopy. Journal of Applied Physics, 2010, 108 (043703), pp.043703. 10.1063/1.3465308 . hal-01760553

HAL Id: hal-01760553
https://hal.science/hal-01760553

Submitted on 6 Apr 2018

HAL is a multi-disciplinary open access archive for the deposit and dissemination of scientific research documents, whether they are published or not. The documents may come from teaching and research institutions in France or abroad, or from public or private research centers.

L'archive ouverte pluridisciplinaire **HAL**, est destinée au dépôt et à la diffusion de documents scientifiques de niveau recherche, publiés ou non, émanant des établissements d'enseignement et de recherche français ou étrangers, des laboratoires publics ou privés.

Depth analysis of boron diffusion in MgO/CoFeB bilayer by x-ray photoelectron spectroscopy

Y. Lu,[1,3,a)] B. Lépine,[2] G. Jézéquel,[2] S. Ababou,[2] M. Alnot,[3] J. Lambert,[4] A. Renard,[4] M. Mullet,[4] C. Deranlot,[1] H. Jaffrès,[1] F. Petroff,[1] and J.-M. George[1]
[1]*Unité Mixte de Physique CNRS/Thales, Campus Polytechnique, 1 Avenue Augustin Fresnel, 91767 Palaiseau, France and Université Paris-Sud, 91405 Orsay, France*
[2]*Equipe de Physique des Surfaces et Interfaces, IPR, UMR 6251, CNRS-Université de Rennes 1, Bâtiment 11C, 35042 Rennes, France*
[3]*Département Physique de la Matière et des Matériaux (P2M), UMR 7198, Institut Jean Lamour, Boulevard des Aiguillettes, BP 239, 54506 Vandœuvre-lès-Nancy, France*
[4]*Laboratoire de Chimie Physique et Microbiologie pour l'Environnement, CNRS UMR 7564, Nancy–Université, 405 rue de Vandœuvre, 54600 Villers-lès-Nancy, France*

(Received 28 February 2010; accepted 17 June 2010; published online 17 August 2010)

We have studied the boron (B) diffusion in MgO/CoFeB bilayer by x-ray photoelectron spectroscopy depth analysis. A large concentration of B (B/Mg=0.16) was found to diffuse into the MgO barrier after 350 °C annealing. The boron in MgO is in a highly oxidized B^{3+} state and is homogenously distributed in the whole barrier. The important B diffusion in MgO could be related to the CoFeB crystallization process which begins from the under CoFeB/Ru interface and pushes boron atoms to diffuse into the MgO barrier during annealing. © *2010 American Institute of Physics*. [doi:10.1063/1.3465308]

I. INTRODUCTION

Magnetic tunnel junctions (MTJs) based on crystalline MgO(001) barrier are now considered as a key for next-generation data storage devices and sensors because of their giant tunneling magnetoresistance (TMR) effect at room temperature.[1,2] Djayaprawira *et al.*[3] have first reported that the polycrystalline CoFeB/MgO/CoFeB based MTJs prepared by magnetron sputtering, which are suitable for mass production, show a TMR larger than 200%. In these MTJs, high temperature annealing is a key factor to obtain high TMR. During annealing the amorphous CoFeB electrode in the as-deposited state becomes crystallized to (001) texture by the MgO barrier.[4] The resulting CoFeB(001)//MgO(001)//CoFeB(001) band structure symmetry is responsible for this giant TMR effect.[5] Due to the low solubility of B atoms in the CoFe matrix (<1%), the crystallization process requires to reject B atoms from the CoFeB layer during the annealing. Recent studies suggest that MgO can act as a sink, absorbing B atoms from the CoFeB layer, and so initiating the crystallization of CoFeB electrode during annealing.[6] Therefore, it is critical to study the B diffusion mechanism and its distribution after annealing. It should lead to a better knowledge of the CoFeB crystallization process which is one of the key parameters for high TMR junctions.

Several groups have studied B diffusion in MgO MTJs by different techniques including x-ray photoelectron spectroscopy (XPS), electron energy-loss spectroscopy (EELS), and three-dimensional atom probe (3DAP) techniques.[6–16] However, different conclusions came out from the experiments. Some groups reported that a considerable quantity of B diffuse into the MgO barrier after annealing,[6–11] while some others observed that boron tends to segregate at the MgO/CoFeB interface and form BO_x after the crystallization of CoFeB layer.[12–15] Moreover, recently, the group of Miyajima *et al.*[16] found that the crystallization of CoFeB layers was strongly dependent on the capping materials. B mainly diffuses to the capping layer and barely to the MgO layer.

In this paper, we present a detailed study of B diffusion and distribution in a MgO/CoFeB bilayer by using XPS depth analysis. It is found that a large concentration of B (B/Mg=0.16) diffuses into MgO barrier rather than being accumulated at the MgO/CoFeB interface after 350 °C annealing. The boron in MgO has a highly oxidized B^{3+} state and it homogenously distributes in the whole barrier. Finally, we will discuss the implication on the CoFeB crystallization process as well as on the nature of the defects in the MgO barrier clarified by our results on B diffusion.

II. EXPERIMENT

We deposited the thin films onto a thermally oxidized Si(001) wafer using a magnetron sputtering system with a base pressure about 5×10^{-8} mbar. The details of the layers in the stack are (in nanometer): substrate/Ta 5/Ru 15/$Ir_{20}Mn_{80}$ 8/$Co_{70}Fe_{30}$ 4/Ru 0.8/$Co_{40}Fe_{40}B_{20}$ 4/MgO 2/Ta 10. The metal layers were deposited under an Ar pressure of 2.5×10^{-3} mbar by dc sputtering, while the MgO layer was deposited by rf sputtering directly from a sintered MgO target under an Ar pressure of 4×10^{-2} mbar. The detailed growth condition can be found elsewhere.[17] The sample is cut into two pieces and one of them is annealed at 350 °C for 1 h in ultrahigh vacuum prior to the XPS depth analysis. XPS analyses were performed under a base pressure of 7×10^{-8} Pa using a VSW Scientific Instruments HA100 spectrometer with a multichannel detection. Al $K\alpha$ (1486.6 eV) was used as the x-ray source. The pass energy of the hemispherical detector was kept at 44 eV. All spectra are refer-

a)Electronic mail: lu@lpm.u-nancy.fr.

 © 2010 American Institute of Physics

Author complimentary copy. Redistribution subject to AIP license or copyright, see http://jap.aip.org/jap/copyright.jsp

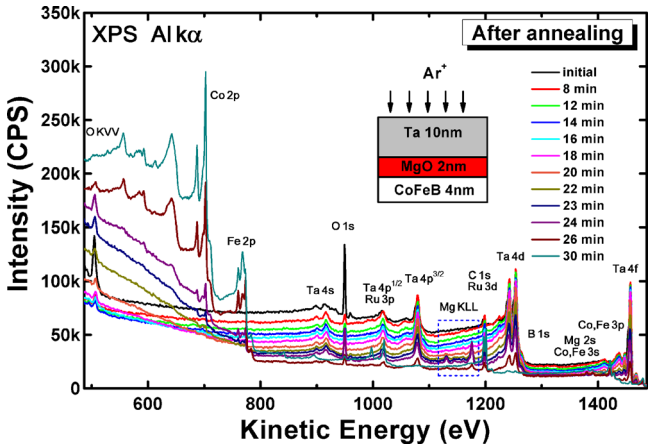


FIG. 1. (Color online) XPS spectra in large scale for the annealed sample after different sputtering time. The inset schematically shows the top structure of the sample.

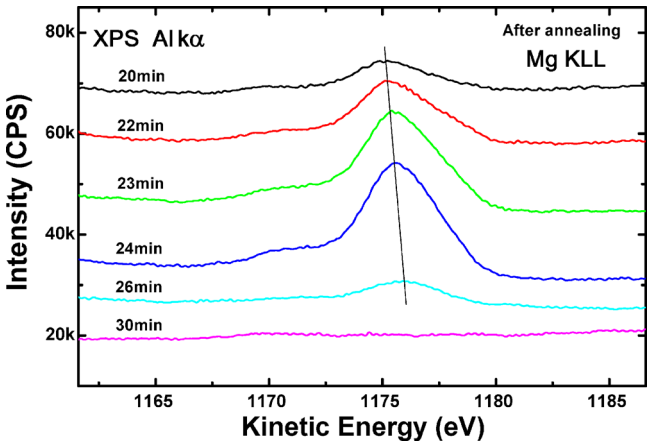


FIG. 2. (Color online) Mg *KLL* spectra of the annealed sample after different sputtering time.

enced to the analyzer Fermi level. Ar^+ ion sputtering (of 4 kV energy) with a rate about 0.4 nm/min was performed to remove the 10 nm Ta protecting layer and carry out the depth analysis. To ensure the homogeneity of ion sputtering, we adopted a 45° incident angle and swept the sample with 1 Hz frequency. Atomic force microscopy measurement reveals that the root-mean square roughness of our sample after Ar^+ sputtering is less than 0.5 nm in a 2×2 μm^2 scan area.

III. RESULTS

A. In-depth analysis and the sensitivity of Mg *KLL* signal

Figure 1 shows the XPS spectra in large scale with different sputtering time. The main peaks have been identified and marked in the figure. Within 26 min of sputtering time, the spectrum features only concern the top three layers in the sample, which is schematically shown in the inset of Fig. 1. In fact, due to the surface oxidation, the top of Ta layer is oxidized to be TaO_x, which is estimated to be 2–3 nm. To carry out the depth analysis, one critical point is how to detect the MgO barrier and control the sputtering depth. Due to the large illumination of the sample and sample holder by x-rays combined both with a slight inhomogeneity of sputtering and redeposition problems on the sample holder, the signals of Ta and oxygen always exists, so they cannot be used to determine the end of the Ta layer for the former or identify the beginning of the MgO layer for the latter signal. We then focus on the signal of Mg. With Al $K\alpha$ x-ray source, four kinds of Mg signals can be collected: Mg 1*s*, Mg *KLL*, Mg 2*s*, and Mg 2*p* with kinetic energy (KE) positions at 176 eV, 1176 eV, 1391 eV, and 1431 eV, respectively. For Mg 1*s*, due to the large difference of KE compared with B 1*s* (KE: 1296 eV), which is used to analyze the B diffusion, the error introduced by the different mean free paths (Mg 1*s*: ~0.8 nm, B 1*s*: ~2.4 nm) (Ref. 18) cannot be negligible. For Mg 2*s* and Mg 2*p*, their signals are relative small and usually are mixed with signals of Fe 3*s* and Fe 3*p* from the under CoFeB layer, respectively. Therefore, they are also not suitable for the detection of the MgO layer. Fortunately, we have found that Mg *KLL* signal is very sensitive to detect the MgO barrier and to control the sputtering depth in the sample, as marked in Fig. 1 with dashed square. Moreover, the KE of Mg *KLL* is close to that of B 1*s*, thus their mean free paths of photoelectron are almost the same, which also favors the depth analysis of B diffusion. Figure 2 shows the spectrum of Mg *KLL* with different sputtering time. It is clearly found that the MgO related Mg *KLL* signal appears after sputtering 20 min and it increases to a maximum after 24 min of sputtering. Then the Mg *KLL* signal quickly decreases at 26 min and disappears at 30 min of sputtering. In addition, a slight shift in about 0.6 eV toward higher KE of this signal was found from 20 to 26 min during sputtering the MgO layer. While the same trend is observed on the B 1*s* "oxide" component (see below), we did not find this shift from the O 1*s* signal nor from the Mg *KLL* signal in the sample studied before annealing (see, Sec. III C). Therefore, this shift might reflect the MgO compositional change near the interfaces.

B. Boron distribution in the MgO barrier

The B 1*s* spectra were also collected from sputtering time 22 to 30 min, as indicated by the Mg *KLL* signal. Because the B 1*s* signal is very weak, we need to increase a lot the scan number and dwell time to increase the signal to noise ratio. After sputtering 22 min to remove the Ta protecting layer, the B 1*s* signal becomes strong enough to be collected. Figure 3(a) shows the B 1*s* spectra after different sputtering time. The energy scale is changed to binding energy (BE) for easy comparison with other results in the literature. The B 1*s* signal from a 50 nm CoFeB sample oxidized by oxygen plasma is also shown in Fig. 3(a) as a reference for the positions of metallic and oxidized B. A Shirley background has been subtracted from all the spectra and their heights are normalized to a constant value. Two components in the B 1*s* spectra can be distinguished. The lower BE one at about 188 eV is assigned to the metallic B from the bottom CoFeB layer. The other peak at about 193 eV can be assigned to the oxidized B in the MgO layer induced by B diffusion from the CoFeB layer. The integrated intensity of each B component, extracted by carefully fitting the B 1*s* spectra, is plotted in Fig. 4 as a function of sput-

Author complimentary copy. Redistribution subject to AIP license or copyright, see http://jap.aip.org/jap/copyright.jsp

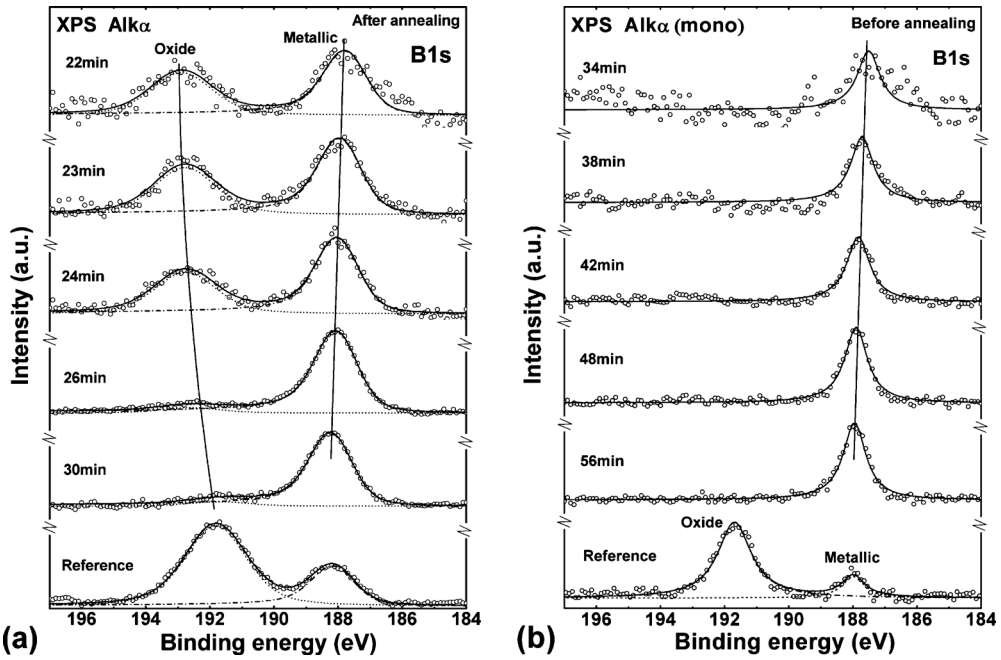


FIG. 3. Depth analysis of B 1*s* spectra after different sputtering time for the samples (a) after annealing and (b) before annealing. The reference sample of a 50 nm oxidized CoFeB layer is shown for comparison.

tering time together with the intensity of the Mg *KLL* signal. It is interesting to find that the intensity evolution of the B oxide component is exactly the same as that of the Mg *KLL* signal. Both signals increase to a maximum at 24 min and then decrease while the metallic B component continues to increase until 26 min. This means that the B oxide is homogeneously distributed in the MgO barrier. On the reverse case, if B oxide was only accumulated at the MgO/CoFeB interface, the B oxide intensity would increase at 26 min instead of decreasing as the same manner as the Mg *KLL* signal.

Further analyzing the peak position in Fig. 3(a), we can find that the position of B oxide between 22 and 24 min sputtering time is almost constant and shifted by about 1 eV to higher BE compared with the B oxide position in the reference sample, which agrees with the results of Read *et al.*[7] The higher BE means that the B in MgO is in a higher oxidation state, closer to B^{3+}, than B of the boron oxide in the oxidized CoFeB layer (BO_x). This B 1*s* position in MgO also agrees with the value measured by Ong *et al.*[19] on B_2O_3 (−193.6 eV with respect to the Fermi level). The shift in B oxide position from 24 to 30 min indicates the change in the distribution of B oxide from inside of the MgO layer to the under CoFeB layer. The B oxide position after 30 min sputtering is found exactly the same as the reference sample. Now we can conclude that even though there might exist a small B oxide proportion at the interface, B oxide is mostly homogeneously distributed in the MgO barrier. Moreover, we found a very slight shift in the position of the metallic B 1*s* component (about 0.2–0.3 eV) to the higher BE side from 22 to 30 min. This position at 30 min sputtering time is also found to be same as the reference sample.

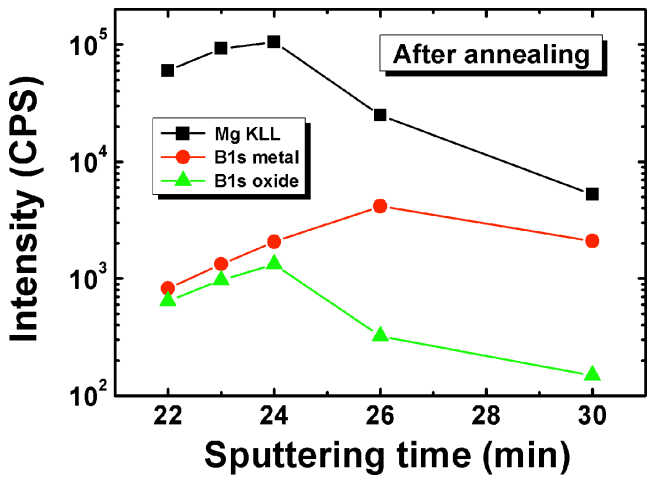


FIG. 4. (Color online) Intensity evolution for Mg *KLL*, B 1*s* metallic and oxide components of the annealed sample after different sputtering time.

C. Depth analysis of the sample before annealing

For the depth analysis, some authors have reported ion radiation-enhanced diffusion (IRED) and segregation up to several nanometers during the Ar^+ sputtering process.[20] If this effect exists in our analysis, i.e., if B diffusion occurs due to sputtering, it could lead to misinterpretation of the results. To check this point, we have also performed the depth analysis in the similar sample before annealing. We have used another XPS system with a KRATOS Axis Ultra electron energy analyzer operating with a monochromatic Al $K\alpha$ source. The sample was sputtered by using a focused Ar^+ beam of 5 kV on a 3×3 mm^2 window to remove the Ta protecting layer. Figure 3(b) shows the B 1*s* spectra after different sputtering time. Nevertheless, the sputtering rate is different from the previous experiment and also the spectrum width is much smaller due to the use of the monochromatic Al $K\alpha$ source. After sputtering 42 min, the Mg *KLL* signal

Author complimentary copy. Redistribution subject to AIP license or copyright, see http://jap.aip.org/jap/copyright.jsp

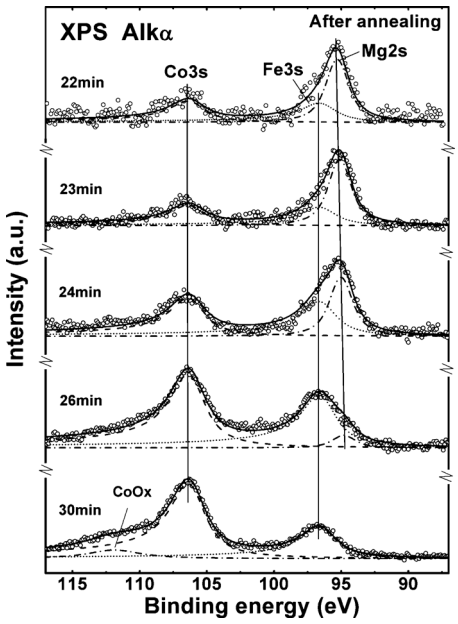


FIG. 5. Deconvolution of Co 3*s*, Fe 3*s*, and Mg 2*s* signals of the annealed sample after different sputtering time.

reaches a maximum, which indicates the sputtering in the MgO layer. The reference sample of oxidized CoFeB is also measured for comparison. Due to charging effect of this strongly oxidized sample, its spectrum has been shifted to obtain the coincidence of the metallic B 1*s* position. It is clearly found that only one metallic B 1*s* component from the bottom CoFeB layer during all sputtering process. This gives a strong argument that the B oxide found in the annealed sample is due to the B diffusion after the annealing. It also rules out the influence of the IRED effect in our samples during sputtering. From the XPS experiment it can be concluded that before annealing, there is no B diffusion in the MgO barrier and very small oxidization at the MgO/CoFeB interface, which is on the contrary to a recent study of B distribution by 3DAP, showing that an important B diffusion occurs even before annealing.[15] Moreover, the metallic B position energy is also shifted in about 0.2–0.3 eV to the higher BE side from 34 to 56 min, in agreement with the result obtained on the sample after annealing. At the moment, we have no definitive explanation for this shift. It cannot be due to the B diffusion in MgO but perhaps to the presence of a small amount of fixed charge (charged defects) in the MgO layer.

D. Determination of the B concentration in the MgO barrier and its distribution in the CoFeB layer

Finally, it is important to quantify the concentration of B that has diffused into the MgO barrier after annealing. Normally, Auger peaks are very broad and they have no regular shape. So it is difficult to estimate the integrated intensity and define the sensitivity factor. Therefore, no sensitivity factor for Mg *KLL* can be found in the XPS database. Here we need to analyze Mg 2*s* signal (Mg 2*p* signal has a strong background influenced by the Ta 4*f* signal), even if it is mixed with the Fe 3*s* signal from the bottom CoFeB layer. Figure 5 shows the deconvolution of Mg 2*s*, Co 3*s*, and Fe 3*s* spectra for different sputtering time. During the fitting procedure, the width and asymmetry of Co 3*s* and Fe 3*s* spectra were fixed to be the same. The intensity and peak position of Mg 2*s* varies according to the Mg *KLL* signal (shown in Fig. 2). After fitting, we can extract the separate contributions of Mg 2*s*, Co 3*s*, and Fe 3*s*.

TABLE I. Estimation of the B diffusion in MgO with the B/Mg ratio for sputtering time from 22 to 24 min.

Sputtering time (min)	B 1*s* oxide (cps·eV)	Mg 2*s* (cps·eV)	B/Mg ratio
22	503	3764	0.158
23	847	6794	0.147
24	1037	7342	0.167

The quantity of B diffusion in the MgO barrier then can be estimated from the data after sputtering 22 to 24 min, as shown in Table I. The ratio of B/Mg is deduced from the areas of the B 1*s* oxide component and Mg 2*s* signal including their corresponding sensitivity factors (B 1*s*: 0.486 and Mg 2*s*: 0.575).[21] The ratio of B/Mg is found to be 0.16 ± 0.01 in the MgO barrier. The relative constant values mean that the B concentration in MgO is almost homogenous.

Moreover, the contribution of Co 3*s* and Fe 3*s* fitted in Fig. 5 allow us to investigate the B distribution in the CoFeB underlayer, which is plotted in Fig. 6 as function of sputtering time by taking account of the corresponding sensitivity factors (Co 3*s*: 0.818, Fe 3*s*: 0.745, and B 1*s*: 0.486).[21] Here the metallic B 1*s* component extracted from the fit in Fig. 3(a) is used for the B concentration in the CoFeB layer. We find a ratio of Co:Fe:B=40:40:20 at the MgO/CoFeB interface after sputtering 22 and 23 min, which is in good agreement with the concentration of the $Co_{40}Fe_{40}B_{20}$ target. With the increase in the sputtering time from 24 to 30 min, the B concentration continuously decreases. It may be attributed to the increase in the signal coming from the $Co_{70}Fe_{30}$ layer which is under the $Co_{40}Fe_{40}B_{20}$ layer because of the mean free path of the x-ray photoelectron.[18] This mean free path effect is clearly seen on the Co/Fe ratio evolution be-

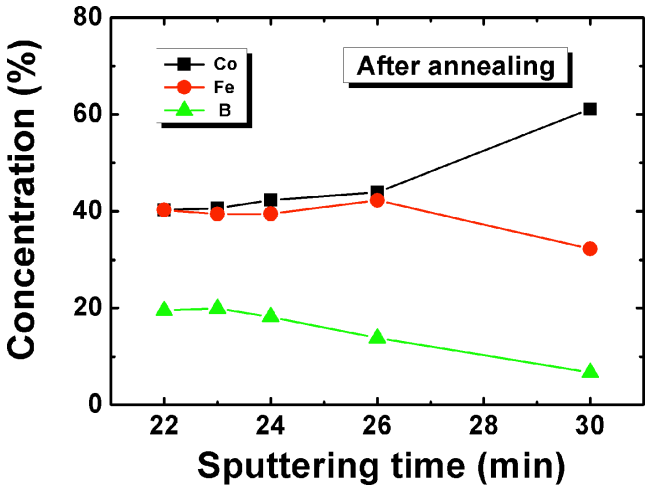


FIG. 6. (Color online) Evolution of the concentration distribution in the CoFeB layer after different sputtering time.

Author complimentary copy. Redistribution subject to AIP license or copyright, see http://jap.aip.org/jap/copyright.jsp

tween 26 and 30 min of sputtering time but not between 24 and 26 min sputtering time. Then, as we will discuss below, the process of crystallization of the CoFeB layer may also play an important role in this boron concentration reduction.

IV. DISCUSSIONS

A. Influence of CoFeB crystallization process to the B diffusion

Our results clearly show that a large concentration of B diffuse into the MgO barrier rather than being accumulated at the CoFeB/MgO interface after annealing at 350 °C. Recently, Miyajima *et al.*[16] studied the crystallization and boron distribution in CoFeB/MgO/CoFeB MTJs by high-resolution transmission electron microscopy and EELS. They have reported that B mainly diffuses to the capping layers and barely to the MgO layers with increasing annealing temperature. The discrepancy of their conclusions with ours may be due to the different crystallization process of the bottom CoFeB electrode. In our previous work,[17] it was observed that the bottom CoFeB electrode in our MTJs is always (011) textured after annealing. However, in the work of Miyajima *et al.*, the top and bottom electrodes are both (001) textured. In fact, the different textures of the bottom CoFeB layer reflect different crystallization processes. The (001) texture means that the crystallization begins at the MgO/CoFeB interface, while the (011) texture indicates that the crystallization starts from the under CoFeB/Ru interface.

This assumption can be highlighted through the analysis of the B distribution in the bottom CoFeB layer as shown in Fig. 6. At the MgO/CoFeB interface, the concentration of B is found to be about 20%, while it decreases with the increase in sputtering time (especially at 26min). Due to the low solubility of B atoms in the CoFe matrix, the crystallization process requires to reject B atoms from the CoFeB layer during annealing.[6] The crystallization from the under CoFeB/Ru side pushes B to diffuse toward the upper MgO barrier. Therefore, a large concentration of B is found in the MgO layer. On the contrary, in Miyajima's work, the crystallization starting from MgO/CoFeB side pushes B toward the under Ru layer, so that few B was found in the MgO barrier. From the view of lattice mismatch, the mismatch of MgO(001)[100]//CoFe(001)[110] (3.7%) is smaller than that of Ru(001)[110]//CoFe(011)[100] (−5.6% in CoFe[100] direction and 15.8% in CoFe[$0\bar{1}1$] direction). It emphasizes the critical role of the MgO/CoFeB interface in competition with the under interface (CoFeB/Ru in our case) to initiate the crystallization of the CoFeB and its influence on the B diffusion.

B. Defects in the MgO barrier

Because boron resides with difficulty in the CoFe matrix,[22] the defects in the MgO barrier seems to be another important factor to accelerate the B diffusion into MgO during annealing. In fact, Read *et al.*[7] and Cha *et al.*[8] have found that B diffusion is very dependent on the growth method. B diffusion is more pronounced in rf-sputtered MgO layers than for *e*-beam evaporated MgO. Generally, for the *e*-beam evaporated MgO, oxygen vacancy is the main defect. In case of sputtered-grown MgO, Mg vacancy also plays an important role.[23] In addition, Choi *et al.*[24] have also evidenced ionic oxygen interstitial defects in the sputtered MgO barrier. We have, therefore, checked the stoichiometry of our MgO barrier with nano-Auger depth analysis (not shown). The ratio of Mg/O is found to be about 0.93, which indicates a small excess of oxygen compared to magnesium. The ratio of Mg/O does not change evidently before and after annealing. This might also explain why B diffusion is so pronounced in our MgO layer.

From our XPS results, we demonstrated that the diffused B inside MgO is in a highly oxidized state (B^{3+}). It leads to two possibilities: (i) B could be in a substitutional position, occupying the Mg vacancies to form a $(MgO)_x(B_2O_3)_y$ compound[11] or (ii) it could be in the amorphous form of B_2O_3 localized in the MgO grain boundaries. The large concentration of B distributed in our MgO layer after annealing agrees both with the claims of Read *et al.*[7] that an intermediate oxide Mg_xB_yO could form after the annealing procedure and with the recent study of boron distribution by Cha *et al.* by using EELS.[11] However, to end up this discussion, further experiments are required. In any case, the large concentration of B species in MgO should introduce a high density of defect states in the MgO band gap[10] and influence the transport property of the CoFeB/MgO/CoFeB MTJs as recently evidenced in our work.[25]

V. CONCLUSION

We have studied the B diffusion in MgO/CoFeB bilayer by XPS depth analysis. Mg *KLL* signal has revealed a very high sensitivity to detect the MgO barrier and to control the sputtering depth. Before annealing, no B species have been found in MgO, while a large concentration of B has diffused into the MgO barrier after 350 °C annealing. The B in MgO has a highly oxidized B^{3+} state and it homogenously distributes in the whole MgO barrier. The B/Mg ratio in MgO is estimated to be 0.16 ± 0.01 by the deconvolution of Co $3s$, Fe $3s$, and Mg $2s$ signals. The important B diffusion in the MgO could be related to the CoFeB crystallization process which begins from the under CoFeB/Ru interface and pushes B into the MgO barrier. In addition, the nonstochiometric MgO barrier before and after annealing, revealing the presence of defects, should also amplify the B diffusion during annealing.

[1] S. S. P. Parkin, C. Kaiser, A. Panchula, P. M. Rice, B. Hughes, M. Samant, and S.-H. Yang, Nature Mater. **3**, 862 (2004).
[2] S. Yuasa, T. Nagahama, A. Fukushima, Y. Suzuki, and K. Ando, Nature Mater. **3**, 868 (2004).
[3] D. D. Djayaprawira, K. Tsunekawa, M. Nagai, H. Maehara, S. Yamagata, N. Watanabe, S. Yuasa, Y. Suzuki, and K. Ando, Appl. Phys. Lett. **86**, 092502 (2005).
[4] S. Yuasa, Y. Suzuki, T. Katayama, and K. Ando, Appl. Phys. Lett. **87**, 242503 (2005).
[5] Y. M. Lee, J. Hayakawa, S. Ikeda, F. Matsukura, and H. Ohno, Appl. Phys. Lett. **89**, 042506 (2006).
[6] T. Takeuchi, K. Tsunekawa, Y. Choi, Y. Nagamine, D. D. Djayaprawira, A. Genseki, Y. Hoshi, and Y. Kitamoto, Jpn. J. Appl. Phys., Part 1 **46**, L623 (2007).
[7] J. C. Read, P. G. Mather, and R. A. Buhrman, Appl. Phys. Lett. **90**, 132503 (2007).

Author complimentary copy. Redistribution subject to AIP license or copyright, see http://jap.aip.org/jap/copyright.jsp

[8]J. J. Cha, J. C. Read, R. A. Buhrman, and D. A. Muller, Appl. Phys. Lett. **91**, 062516 (2007).
[9]J. Schmalhorst, A. Thomas, G. Reiss, X. Kou, and E. Arenholz, J. Appl. Phys. **102**, 053907 (2007).
[10]S. S. Mukherjee, D. MacMahon, F. Bai, C.-L. Lee, and S. K. Kurinec, Appl. Phys. Lett. **94**, 082110 (2009).
[11]J. J. Cha, J. C. Read, W. F. Egelhoff, Jr., P. Y. Huang, H. W. Tseng, Y. Li, R. A. Buhman, and D. A. Muller, Appl. Phys. Lett. **95**, 032506 (2009).
[12]J. Y. Bae, W. C. Lim, H. J. Kim, T. D. Lee, K. W. Kim, and T. W. Kim, J. Appl. Phys. **99**, 08T316 (2006).
[13]Y. Jang, C. Nam, K.-S. Lee, B. K. Cho, Y. J. Cho, K.-S. Kim, and K. W. Kim, Appl. Phys. Lett. **91**, 102104 (2007).
[14]C. Y. You, T. Ohkubo, Y. K. Takahashi, and K. Hono, J. Appl. Phys. **104**, 033517 (2008).
[15]S. Pinitsoontorn, A. Cerezo, A. K. Petford-Long, D. Mauri, L. Folks, and M. J. Carey, Appl. Phys. Lett. **93**, 071901 (2008).
[16]T. Miyajima, T. Ibusuki, S. Umehara, M. Sato, S. Eguchi, M. Tsukada, and Y. Kataoka, Appl. Phys. Lett. **94**, 122501 (2009).
[17]Y. Lu, C. Deranlot, A. Vaurès, F. Petroff, J.-M. George, Y. Zheng, and D. Demailles, Appl. Phys. Lett. **91**, 222504 (2007).
[18]M. P. Seah and W. A. Dench, Surf. Interface Anal. **1**, 2 (1979).
[19]C. W. Ong, H. Huang, B. Zheng, R. W. M. Kwok, Y. Y. Hui, and W. M. Lau, J. Appl. Phys. **95**, 3527 (2004).
[20]K. Neubeck, C.-E. Lefaucheur, H. Hahn, A. G. Balogh, H. Baumann, K. Bethge, and D. M. Rück, Nucl. Instrum. Methods Phys. Res. B **106**, 589 (1995).
[21]J. H. Scofield, J. Electron Spectrosc. Relat. Phenom. **8**, 129 (1976).
[22]J. D. Burton, S. S. Jaswal, E. Y. Tsymbal, O. N. Mryasov, and O. G. Heinonen, Appl. Phys. Lett. **89**, 142507 (2006).
[23]P. G. Mather, J. C. Read, and R. A. Buhrman, Phys. Rev. B **73**, 205412 (2006).
[24]Y. S. Choi, Y. Nagamine, K. Tsunekawa, H. Maehara, D. D. Djayaprawira, S. Yuasa, and K. Ando, Appl. Phys. Lett. **90**, 012505 (2007).
[25]Y. Lu, M. Tran, H. Jaffrès, P. Seneor, C. Deranlot, F. Petroff, J.-M. George, B. Lépine, S. Ababou, and G. Jézéquel, Phys. Rev. Lett. **102**, 176801 (2009).

Author complimentary copy. Redistribution subject to AIP license or copyright, see http://jap.aip.org/jap/copyright.jsp